

**Proceedings of the 13th AUN/SEED
NET Regional Conference on Materials
(RCM 2020) and the 1st International
Conference on Materials Engineering
and Manufacturing (ICMEM 2020)**

The publishing information for this conference proceedings is as follows:
AIP Conference Proceedings, Vol. 5200, No. 1, May 2020, ISBN 978-0-7354-4000-0,
Manufactured in the USA, May 2020 and available online at <https://doi.org/10.1063/1.5134444>



**RCM-ICMEM
2020**



Issues

Select Decade 2020 ▾

Select Year 2021 ▾

Issue 11 November - Volume 2338, Issue 1 ▾

PRELIMINARY

Preface: 13th AUN/SEED-Net Regional Conference on Materials 2020 (RCM 2020) and 1st International Conference on Materials Engineering and Manufacturing (ICMEM 2020) 🛒

AIP Conference Proceedings 2338, 010001 (2021) doi:
<https://doi.org/10.1063/12.0006002>

[View article](#)

[PDF](#)

Committees: 13th AUN/SEED-Net Regional Conference on Materials 2020 (RCM 2020) and 1st International Conference on Materials Engineering and Manufacturing (ICMEM 2020) 🛒

AIP Conference Proceedings 2338, 010002 (2021) doi:
<https://doi.org/10.1063/12.0006803>

[View article](#)

[PDF](#)

RCM

Geometrical effect of SPCC bar by twisting test using graded load 🛒

[Gusti Putu Surya Govinda Atmaja](#); [Kresna Budiman](#); [Rachmadi Norchayo](#); [Heru Santoso B. Rochardjo](#); [I. Gusti Ketut Puja](#); [Muhammad Akhsin Muflikhun](#)

AIP Conference Proceedings 2338, 020001 (2021) doi:
<https://doi.org/10.1063/5.0066988>

[Abstract ▾](#)

[View article](#)



Modeling of the bridge support based on carpenter tape geometry

Raihan Qolby Santoso; Gil Nonato C. Santos; Alvin Y. Chua; Muhammad Akhsin Muflikhun

AIP Conference Proceedings 2338, 020002 (2021) doi:
<https://doi.org/10.1063/5.0066995>

Abstract 

View article

 PDF

Effect of Ceric (IV) ammonium nitrate concentration on preparation and characterization of chitosan-graft-maleic anhydride as potential drug delivery system

Milla Nadia; Yuni Kusumastuti; Sang K. Wirawan; Daniel Timotius

AIP Conference Proceedings 2338, 020003 (2021) doi:
<https://doi.org/10.1063/5.0067872>

Abstract 

View article

 PDF

Effects of notch geometry on stress, strain, and safety factor of bimetal and fiber-metal laminates under charpy impact test using explicit dynamic model

Wisnu Hozaifa Hasan; Tegar Fisabilillah; Jayan Sentanuhady; Muslim Mahardika; Muhammad Akhsin Muflikhun

AIP Conference Proceedings 2338, 020004 (2021) doi:
<https://doi.org/10.1063/5.0066999>

Abstract 

View article

 PDF

Effects of angle in notch geometry on stress, safety factor, and displacement of SPCC plate under tension loading

Justin Edwardo; Ari Permana; Muhammad Akhsin Muflikhun

AIP Conference Proceedings 2338, 020005 (2021) doi:
<https://doi.org/10.1063/5.0067002>

Abstract 

View article

 PDF

Comparison on the mechanical strength properties of nickel slag-based geopolymer versus Portland cement-concrete: Compressive and flexural strength 🛒

[Emir Kharisma Firdaus](#); [Rowi Alfata](#); [Sotya Astutiningsih](#); [Nuraziz Handika](#)

AIP Conference Proceedings 2338, 020006 (2021) doi:
<https://doi.org/10.1063/5.0070903>

[Abstract](#) ▾

[View article](#)

[PDF](#)

Corrosion in geothermal facilities: Their causes, effects, mitigation, and worldwide cases 🛒

[Khasani](#); [Kusmono](#); [Pri Utami](#); [Rachmawan Budiarto](#)

AIP Conference Proceedings 2338, 020007 (2021) doi:
<https://doi.org/10.1063/5.0066755>

[Abstract](#) ▾

[View article](#)

[PDF](#)

A first principles study on aluminium-sulfur co-doped graphene as an electro-catalyst for oxygen reduction reaction in a PEM fuel cell 🛒

[Christabel Ngetich](#); [Evan Wanjiru](#); [Kabini Karanja](#); [Patrick Kareru](#); [James Mutua](#)

AIP Conference Proceedings 2338, 020008 (2021) doi:
<https://doi.org/10.1063/5.0066645>

[Abstract](#) ▾

[View article](#)

[PDF](#)

ICMEM-MANUFACTURING

Fused deposition modelling for the fabrication of metal oxide based gas sensor 🛒

[Wangi Pandan Sari](#); [Samuel Agbroko](#); [James Covington](#)

AIP Conference Proceedings 2338, 030001 (2021) doi:
<https://doi.org/10.1063/5.0067327>

[Abstract](#) ▾

[View article](#)

[PDF](#)

Pathways to improve new product design cost effectiveness and time to market speed using integrated collaborative product design concept: A critical review

Muhammad Shodiq Abdul Khannan; Muhammad Kusumawan Herliansyah; Andi Sudiarso

AIP Conference Proceedings 2338, 030002 (2021) doi: <https://doi.org/10.1063/5.0068229>

Abstract 

View article

 PDF

Solar powered-automatic yarn winding machine

Sumartini Dana; Ade Manu Gah; Maychel G. Pae

AIP Conference Proceedings 2338, 030003 (2021) doi: <https://doi.org/10.1063/5.0068363>

Abstract 

View article

 PDF

Low-cost supervisor and servant for Covid-19 patients based on cloud computing

Zakaria Sembiring; Enda Yunita Surbakti; Jenni Veronika Ginting; Harianta Sembiring

AIP Conference Proceedings 2338, 030004 (2021) doi: <https://doi.org/10.1063/5.0066756>

Abstract 

View article

 PDF

Optimization of removal impurities from Fe element in concentrate rare earth elements sulfate coal of fly ash with Response Surface Methodology (RSM)

Rizki Istinanda; Himawan Tri Bayu Murti Petrus; Agus Prasetya

AIP Conference Proceedings 2338, 030005 (2021) doi: <https://doi.org/10.1063/5.0066648>

Abstract 

View article

 PDF

The influence of machining parameters using cryogenic cooling system

Arie Yudha Budiman; Amrifan Saladin Mohruni; Safian Sharif; Aneka Firdaus; Bima Satria Nugraha

AIP Conference Proceedings 2338, 030006 (2021) doi: <https://doi.org/10.1063/5.0070884>

[Abstract](#) [View article](#)[PDF](#) 

ICMEM-MATERIALS

The failure analysis of a leak-off oil pipe ASTM A106 on compact separator at an offshore facility 

[Ari Antono](#); [Ade Irawan](#); [Badrul Munir](#)

AIP Conference Proceedings 2338, 040001 (2021) doi:
<https://doi.org/10.1063/5.0066664>

[Abstract](#) [View article](#)[PDF](#) 

Quantitative risk assessment for external corrosion of buried onshore pipeline by using direct examination 

[Yanita Firda Adelia](#); [Richard Manurung](#); [Hafidz Permana](#); [Badrul Munir](#)

AIP Conference Proceedings 2338, 040002 (2021) doi:
<https://doi.org/10.1063/5.0066688>

[Abstract](#) [View article](#)[PDF](#) 

A failure analysis study on the flange of submersible vertical pump ASTM A234 operated in offshore platform 

[Arif Cahyono](#); [Ade Irawan](#); [Badrul Munir](#)

AIP Conference Proceedings 2338, 040003 (2021) doi:
<https://doi.org/10.1063/5.0066655>

[Abstract](#) [View article](#)[PDF](#) 

The microwave activation effect on the surface morphology of activated charcoal from *Arenga pinnata merr* bunches 

[Nanang Adrianto](#); [Andi Marwanti Panre](#); [Rivaldo Marsel Tumbelaka](#); [Muhammad Anas](#)

AIP Conference Proceedings 2338, 040004 (2021) doi:
<https://doi.org/10.1063/5.0066654>

[Abstract](#) [View article](#)[PDF](#) 

Experimental of diametral tensile strength, compressive strength and vickers hardness of hydroxyapatite/zirconia (HAp/ZrO₂) composites as a candidate of dental prostheses 🗑

[M. Aisya Fatima Sampurno](#); [Muhammad Waziz Wildan](#)

AIP Conference Proceedings 2338, 040005 (2021) doi:
<https://doi.org/10.1063/5.0068004>

[Abstract](#) ▾

[View article](#)

[PDF](#)

Synthesis of solid activator for geopolymer product from fly ash and sodium hydroxide 🗑

[Okti Ulandari](#); [Widi Astuti](#); [Slamet Sumardi](#); [Agus Prasetya](#); [Himawan Tri Bayu Murti Petrus](#)

AIP Conference Proceedings 2338, 040006 (2021) doi:
<https://doi.org/10.1063/5.0066649>

[Abstract](#) ▾

[View article](#)

[PDF](#)

The corrosion study of 90Cu-10Ni (UNS C70600) materials in ammonia and sulfide environments 🗑

[Husaini Ardy](#); [Firmansyah Sasmita](#); [Efvan Adhe Putra Pradana](#)

AIP Conference Proceedings 2338, 040007 (2021) doi:
<https://doi.org/10.1063/5.0066757>

[Abstract](#) ▾

[View article](#)

[PDF](#)

Preparation and characterization of nano crystal cellulose from oil palm trunk for adsorption of methylene blue 🗑

[Fahmi Fathurrahman Miranda](#); [Aristawati Sekar Putri](#); [Mega Mustikaningrum](#); [Ahmad Tawfiequrrahman Yuliansyah](#)

AIP Conference Proceedings 2338, 040008 (2021) doi:
<https://doi.org/10.1063/5.0067128>

[Abstract](#) ▾

[View article](#)

[PDF](#)

Inflammability of GFRP composite with the addition of aluminum tri-hydroxide, boric acid, and sodium silicate 🗑

[Macuk Susilo](#); [Wijang Wisnu Raharjo](#); [Kuncoro Diharjo](#)

AIP Conference Proceedings 2338, 040009 (2021) doi:
<https://doi.org/10.1063/5.0067006>

[Abstract](#) [View article](#)[PDF](#) 

Cathodic protection design of high voltage tower in offshore for 20 years service life

[Dian Sumantri](#); [Priyo Tri Iswanto](#); [Muhammad Faishal Fakhri Wibowo](#)

AIP Conference Proceedings 2338, 040010 (2021) doi:
<https://doi.org/10.1063/5.0068080>

[Abstract](#) [View article](#)[PDF](#) 

Design of crude oil tank cathodic protection in onshore for 20 years service life

[Dian Sumantri](#); [Priyo Tri Iswanto](#)

AIP Conference Proceedings 2338, 040011 (2021) doi:
<https://doi.org/10.1063/5.0068079>

[Abstract](#) [View article](#)[PDF](#) 

Effects of initial precursors on calcium titanate perovskite formation using mechanochemical method

[Alvin Muhammad Habieb](#); [Anawati Anawati](#)

AIP Conference Proceedings 2338, 040012 (2021) doi:
<https://doi.org/10.1063/5.0066659>

[Abstract](#) [View article](#)[PDF](#) 

High electrochemical performance of Al-doped $\text{Li}_4\text{Ti}_5\text{O}_{12}$ (LTO) with prepared via sol-gel route at low pH as anode for lithium ion battery

[Slamet Priyono](#); [Bambang Prihandoko](#); [Akhmad Herman Yuwono](#)

AIP Conference Proceedings 2338, 040013 (2021) doi:
<https://doi.org/10.1063/5.0068322>

[Abstract](#) [View article](#)[PDF](#) 

ZnO-Ag nanoparticles produced via two-step pulsed laser ablation in liquid (PLAL) as antibacterial agent against *Staphylococcus aureus*

[Nurfina Yudasari](#); [Rahma Anugrahwidya](#); [Maria Margaretha Suliyanti](#); [Dahlang Tahir](#); [Cuk Imawan](#); [Dede Djuhana](#)

AIP Conference Proceedings 2338, 040014 (2021) doi:
<https://doi.org/10.1063/5.0067874>

[Abstract](#) ▾

[View article](#)

[PDF](#)

Design of impressed current cathodic protection of offshore platform in East Borneo Sea 🛒

[Andi Wiryawan](#); [Priyo Tri Iswanto](#)

AIP Conference Proceedings 2338, 040015 (2021) doi:
<https://doi.org/10.1063/5.0068078>

[Abstract](#) ▾

[View article](#)

[PDF](#)

Pipe stress simulation and failure analysis of carbon steel flange spool in CO₂ gas flow condition 🛒

[Laksmna Putra Leuvinadrie](#); [Johny Wahyuadi M. Soedarsono](#)

AIP Conference Proceedings 2338, 040016 (2021) doi:
<https://doi.org/10.1063/5.0070886>

[Abstract](#) ▾

[View article](#)

[PDF](#)

Failure analysis under tensile loading of a structural material by acoustic emission technique 🛒

[Arif Abdullah Rashid](#); [Tawhidul Islam Khan](#)

AIP Conference Proceedings 2338, 040017 (2021) doi:
<https://doi.org/10.1063/5.0066898>

[Abstract](#) ▾

[View article](#)

[PDF](#)

The effectivity of pre-treatment process of recycled HDPE based on the mechanical recycling method 🛒

[Aisha Nurtabina](#); [Azwar Manaf](#); [Masayu E. Hafizah](#); [Andreas](#)

AIP Conference Proceedings 2338, 040018 (2021) doi:
<https://doi.org/10.1063/5.0067941>

[Abstract](#) ▾

[View article](#)

[PDF](#)

Utilization of corn husk for tissue papermaking 🛒

[Natalia Suseno](#); [Marisca E. Gondokesumo](#); [Puspita R. Permatasari](#)

[Abstract](#) ▾

[View article](#)

[PDF](#)

Effect of non-isothermal aging on microstructure and impact toughness of Al–Si–Cu–Fe cast alloy

[Apang Djafar Shieddieque](#); [Shinta Virdhian](#); [Moch Iqbal Zaelana Muttahar](#); [Jatira](#); [M. Rizal Akbar](#); [Ghalib Dwi Kanestu](#)

AIP Conference Proceedings 2338, 040020 (2021) doi:
<https://doi.org/10.1063/5.0066662>

[Abstract](#) ▾

[View article](#)

[PDF](#)

Mangrove (*Rhizophora mucronata*) leaves extract as steel corrosion inhibitor

[Arif Wahyudianto](#); [Andrian Fernandes](#); [Wajilan](#)

AIP Conference Proceedings 2338, 040021 (2021) doi:
<https://doi.org/10.1063/5.0068272>

[Abstract](#) ▾

[View article](#)

[PDF](#)

A thermal insulator manufacturing, using solid residuals from pulp and paper factories in Missan City

[Waleed Khalaf Jabbar Allamy](#); [Ibrahim Ali Hameed Al-Najati](#)

AIP Conference Proceedings 2338, 040022 (2021) doi:
<https://doi.org/10.1063/5.0067247>

[Abstract](#) ▾

[View article](#)

[PDF](#)

Effect of electrode type and salt addition to ionized water to prepare alkaline water

[Eko Handoko](#); [Agus Prasetya](#); [Indra Perdana](#)

AIP Conference Proceedings 2338, 040023 (2021) doi:
<https://doi.org/10.1063/5.0067065>

[Abstract](#) ▾

[View article](#)

[PDF](#)

Fabrication and tensile properties of ABS/cellulose nanocrystal nanocomposite filaments for 3D printing 🛒

Kusmono; Pramono Permata Aji

AIP Conference Proceedings 2338, 040024 (2021) doi:
<https://doi.org/10.1063/5.0066895>

[Abstract](#) ▾

[View article](#)

[PDF](#)

Failure analysis of wet solvent stainless steel pipe 🛒

Hendy Setiawan; Johny Wahyuadi Mudaryoto

AIP Conference Proceedings 2338, 040025 (2021) doi:
<https://doi.org/10.1063/5.0066670>

[Abstract](#) ▾

[View article](#)

[PDF](#)

Geometrical Effect of SPCC Bar by Twisting Test Using Graded Load

Gusti Putu Surya Govinda Atmaja¹, Kresna Budiman¹, Rachmadi Norchayo¹, Heru Santoso B Rochardjo¹, I Gusti Ketut Puja² and Muhammad Akhsin Muflikhun^{1, a)}

¹ *Department of Mechanical and Industrial Engineering, Faculty of Engineering, Universitas Gadjah Mada, Jl. Grafika No. 2, Yogyakarta 55281, Indonesia*

² *Department of Mechanical Engineering, Sanata Dharma University, Yogyakarta, Indonesia*

^{a)} Corresponding author: akhsin.muflikhun@ugm.ac.id

Abstract. This study presented the geometrical effect of the SPCC bar by twisting the test using a graded load. For the first time, the geometrical effect of the SPCC bar was simulated and studied. The SPCC bar with the same mass and various cross-section were simulated, studied, and compared. The study also simulated the SPCC bar with the same cross-sectional width, but with various cross-sectional geometry. The ASTM F1264-16 guidelines were referred to and applied for the basic dimension of the specimens for the twisting test. Simulation analysis was conducted for various cross-sectional geometry of the SPCC bar. The Von-Mises stress, displacement, and safety factor of various cross-sectional geometry were presented in this study. We analyzed the location of the maximum stress and minimum safety factors. Differences in the cross-sectional geometry of the SPCC bar showed various behavior that tends to show different analysis. From this study, it appears that rounder bars had lower von mises stress value and displacement and had higher safety factors compared to other cross-sectional geometry.

INTRODUCTION

In various industry, steel was and is still one of the most essential material, especially in an automotive and structural application. Recently, concrete-filled steel, tubular steel, and circular tube steel are used in many structural applications, automotive applications, and even the spaceship application. These massive steel applications are due to the high elongation and high initial stiffness compared to metal-based material. In a recent study, the steel material showed high compatibility with composites, such as CFRP, and had huge potential applications in various industries [1-5].

Multitude of studies has been reported about torsion or twisting test related to the mechanical properties and material behaviour under given torsional load. A study conducted by Ju et al. [6] develops analytical approaches to estimate the torsional behaviour of steel fibre reinforced concrete. This study considered two approaches that eventually confirmed by a series of experiment and simulations. This research showed both approaches (composite material model) and (Direct tension transfer models) were working together to provide a well-explained behaviour of the SFRC. Another study by Rao et. al. [7] also built an analytical model of SFRC when subjected to pure tension. In this study, the model to predict torque-twist of SFRC member subjected to torsional load is proposed by considering the softening effect of the concrete. The resulting model proved to reasonably estimates the torsional behaviour of the SFRC bar under torsional loading.

In simulation and optimization of the structural application, the torsional or twisting test was also reasonably considered. Study form Han et. al. [8] study the performance of concrete-filled thin-walled steel tubes (CFST) subjected to pure torsional load. The study conducted using FES simulation tool ABAQUS to determine the ultimate torsional strength of the concrete-filled thin-walled steel tubes and comparing it to the actual test result. The resulting simulation proved to give a reasonable estimation of the performance and behaviour of CFST. Another study from Wang et al. [9] aiming to optimize the honeycomb sandwich beam-bar subjected to torsion test. The paper aims to

maximize torsional capacities of such structure. The resulting optimization showed that the sandwiched honeycomb structure had a relatively good impact on the overall bending capacities.

Cao et al. [10] investigated the complex torsional analysis with higher complexities and multiple loads. This study presented proven computational modelling for studying the performance of steel-concrete columns under combined compression-bending-shear-torsion. Considering torsion provided by ABAQUS. Cao et al. verified the computational model experimentally by using many considerations, such as the effect on the torsional action of steel-concrete pillars of the axial load ratio, torsion-bending concrete strength, steel ratio, longitudinal reinforcement ratio, stirrup ratio, and shear-span ratio. With increasing concrete strength and declining shear-span ratio, the column's initial torsion stiffness and ultimate torsion strength are seen to increase. Moreover, the most influential parameter for determining the steel-concrete column's ultimate torsion was the steel ratio.

Another research considering complex torsional analysis conducted by Cui et al. [11]. Here the molecular dynamics of twist grain boundaries of copper under uniaxial tension are analyzed. The research included calculating and observing grain boundary, especially for its role in shaping the materials' mechanical properties. This research concluded that the materials' mechanical properties could be enhanced with increasing the twist angle for the <001> and <101> twist GD structure. Research by Hu et al. [12] also considers the complex torsional analysis of mechanical strengthening of CNT ribbon by considering interface and boundary conditions. The research observed the microstructural evolution, and the accompanying strengthening effect of the carbon CNT assemblies. This research concludes that strengthening mechanism of CNT ribbon was applicable.

The above explanation gives a reasonable consideration of the torsional test for a particular material, especially material used in the automotive and structural application. The research from Meram et al. [13] viewed the screwed joint capabilities of CFRP laminates through quasi-static torsion and compression test. This research has further shown geometry, Helicoil reinforced ones, have higher torsional and compressional capabilities than other materials.

In the structural application, plentiful research about the torsional test was conducted to determine the torsional capabilities of the structural element. The research from Pi et al. [14] observed the seismic behaviour of concrete-filled steel tubular columns with internal H-section under pure torsion and compression test. This research studied the torsional properties and seismic behaviour of widely used material concrete-filled steel tube columns. The research provided understanding from the torsional properties of steel tubular columns with H-section under the pure torsion and compression employing multitude calculations and analysis of previous studies. Another study from Yogo et al. [15] studied the stress-strain curve using high-pressure torsion test. This study proved the importance of torsional test for determining mechanical properties of materials. This test was conducted to observed mechanical behaviour of aluminium alloy and carbon steel under high strain. The result showed that mechanical properties obtained by this method have lower uncertainties than traditional method under the large strains condition.

Research from Alabdulhady et al. [16], Hadhood et al. [17], Siddiqui et al. [18] all considers the torsional properties of different materials. Alabdulhady et al. studied the torsional behaviour of RC beams strengthened with PBO-FCRM. This research concluded that the strengthened of PBO-FCRM could promote additional resistance to torsional loading. Research from Hadhood et al. [17] considers torsional condition in concrete beams with GFRP spirals. The research showed that the spiral reinforced concrete beams perform relatively well under the tensional test. Other research conducted by Shiddiqui et al. studied the torsional properties off Carbon fibre reinforced epoxy composites containing carbon nanotubes. This research conducted using CFRE with the addition of 0,5%wt CNTs. The research showed a significantly positive correlation between CNTs and shear strength at 0,5%wt. However further increases on CNTs concentrations would lead to agglomeration of CNT content, thus expressed negative effect on torsional properties

Moreover, there was research for obtaining and studying SPCC and steel-related material. Muflikun et al. [1, 19-12] studied SPCC material combined with CFRP under various loading in various applications. The research was conducted using SPCC variously combined with CFRP to study its failure mode under axial and flexural loading. This research proved that SPCC-CFRP composite laminates have better axial and flexural loading properties. Research from McClafllin et al. [21] investigated torsional deformation and fatigue behaviour of solid and thin-walled tube specimens made of a high strength quenched and tempered spring steel. The research used prediction from the von Mises and Tresca criteria and actual data to compare the result. The experiment has shown that von Mises and Tresca criteria were valid to some extent. The failure of von Mises and Tresca prediction was proposed because of the homogeneity assumption of the material used.

However, the research studying the geometrical effect of tensile loading in SPCC is limited to some extend Research from Hassani et al. consider the analysis of saint-venant torsion in a rectangular bar 22 and cracked-bar with coating layer 23. Although considered the geometrical properties, these two research did not consider the general effect of various geometry in shaping steel behaviour, especially the SPCC bar, under torsional loading. The research

concerned about the analysis of saint-venant torsion and cracked-bar with coating in response to the torsional stress. The result presented the behaviour and predicted behaviour of rectangular steel bar under torsional loading.

Eventually, it can be seen despite the multitude of tests on torsional properties. None of them studied the geometrical effect of the Steel Plate Col Commercial JIS G3141 (SPCC) bar using a graded load. This research aims to develop and studied the effect of cross-sectional geometries of the SPCC bar on the maximum stress or von mises stress, maximum deformations, and the safety factor across the SPCC bar. The research also aimed to search for optimal cross-sectional geometry for the structural application. This research will be conducted using Finite Element Analysis Software ANSYS. The SPCC bar will be modelled and correctly constrained with respect to ASTM F1264-16 standard for static torsional testing. This research also presents and compares the theoretical calculation and result of the simulations.

METHODS AND MATERIALS

Material

The material used in the present study is Steel Plate Col Commercial JIS G3141 (SPCC). The properties of the materials are obtained from the previous study[20, 24-25]. The properties of the SPCC are presented in table 1.

TABLE 1. Mechanical Properties of SPCC

Mechanical Properties	Value	Unit
Thermal Conductivity	5.60 E+01	$W/(m \cdot ^\circ C)$
Specific Heat	4.80 E+02	$J/(kg \cdot ^\circ C)$
Thermal Expansion Coefficient	1.10 E-05	$inv/^\circ C$
Behaviour	Isotropic	
Young's Modulus	2.17 E+11	Pa
Poisson's Ratio	0.35	
Shear Modulus	8.00 E+10	Pa
Density	7.85 E+03	kg/m^3
Yield Strength	2.30 E+08	Pa
Tensile Strength	3.45 E+08	Pa

Method

The study is conducted using Finite Element Analysis Software ANSYS R2 2020 Student Edition. The SPCC bar with specific geometry was modelled and simulated. There is four cross-sectional geometry that was tested and simulated. The corresponding geometry was triangular, square, hexagonal, and circular. Each cross-sectional geometry had two specimens, one with the same mass value and another with the same cross-sectional width or diameter length. The length of all specimens was 230 mm. Other geometrical factors of each shape are shown in Fig.1 and Fig. 2

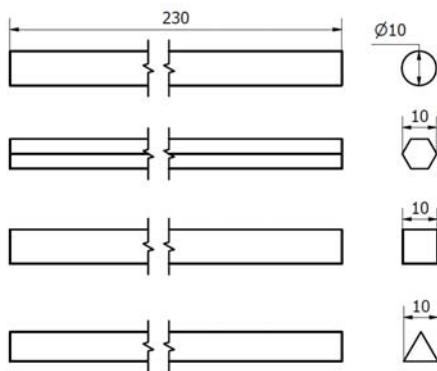


FIGURE 1. Engineering drawing of same cross-sectional width-length SPCC bar

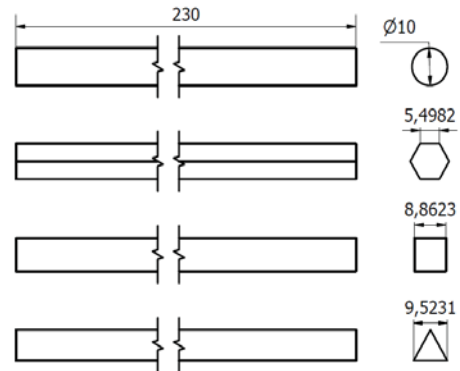


FIGURE 2. Engineering drawing of equal-mass SPCC bar

Each of the cross-sectional geometry was simulated twice. The first simulation is done in each geometry with identical mass value. The second simulation was done in each geometry with identical width and diameter length. Both simulations referred to the ASTM F1264-16 standard for static torsional testing [26]. Before the finite element analysis simulation, all of the specimens were constrained on the longitudinal edge surface, we set the other surface with a set value of torsion. The torsion was varied from 1, 3, 5, 10, 15, 20, 23, 25, and 30 Nm. We applied all value of torsion to each sample. After the simulation finished, the value of von mises stress, safety factor, and displacement of each specimen was captured. The highest stress, longest displacement, and lowest safety were obtained and recorded.

The value of the maximum torsional stress of each specimen was also calculated. The value was calculated using Microsoft Office Excel 365. The formula for calculating the maximum torsional stress is presented below [27-28].

$$\tau_{max} = \frac{Tc}{J} \quad (1)$$

Here, T correspond to the value of torque applied, c represents the distance from the bar's axis to the outermost point in the bar's cross-section, and J represent the value of polar moment inertia of the bar. The formula for calculating polar moment inertia are presented below[27-28],

$$J = \int \rho^2 dA \quad (2)$$

Here, ρ represents the distance of the small element from the bar's axis and dA represents an incremental area. **Table 2.** Showed the calculated polar moment of inertia of each cross-sectional geometry [27-28]. With s refer to the length of the side of each geometry and d referred to the diameter of the circle. Combining the formula for the polar moment inertia in **table 2** and the first equation, the formula for calculating the maximum stress achieved in the SPCC bar is presented in **table 2**. Calculation for safety factor and maximum twist displacement is shown in **table 2** [27-28].

TABLE 2. Polar moment inertia, maximum stress, safety factor, and maximum twist displacement of SPCC bar of each geometry [27-28]

Cross-Sectional Geometry	Polar Moment of Inertia	Maximum Stress	Safety Factor	Maximum Twist Displacement
Circular	$\frac{\pi d^4}{32}$	$5.09 \frac{T}{d^3}$	$\frac{16T}{\pi d^3 \sigma_Y}$	$\frac{8TL}{\pi d^3 G}$
Triangular	$\frac{\sqrt{3}}{48} s^4$	$20 \frac{T}{s^3}$	$20 \frac{T}{\sigma_Y s^3}$	$46 \sqrt{3} \frac{TL}{3Gs^3}$
Square	$\frac{s^4}{6}$	$4.81 \frac{T}{s^3}$	$4.81 \frac{T}{\sigma_Y s^3}$	$7.10 \frac{TL}{Gs^3}$
Hexagonal	$\frac{5\sqrt{3}}{8} s^4$	$0.92 \frac{T}{s^3}$	$0.92 \frac{T}{\sigma_Y s^3}$	$0.92 \frac{TL}{Gs^3}$

Here, σ_Y represents the yield stress of the SPCC.

RESULTS

Various Cross-Sectional Geometry with Equal Mass

The simulation data with the equal-mass condition is presented in **Figure 3(a)-(c)**. Figure 3 (a) shows that the triangular bar showed the highest stress than other geometry bars. The results showed that square bar, hexagonal bar, and circular bar show no significant difference. In small torque, i.e., 5 Nm, there are similar results between these three bars. However, for the triangular bar, the results are more than 200 MPa compared to other bars with less than 100 MPa. **Figure 3 (b)** illustrated the safety factor of different bars. It is shown that the safety factor on small loads (i.e., 5 Nm) of the square, hexagonal, and circular bar has a small difference. Still, the triangular bar has a substantial difference in safety factor compared to all other geometries. **Figure 3 (c)** illustrated the displacement or deformation of the bars. It is shown that the square, hexagonal, and circular rod has a small difference in displacement, with a circular shape having the lowest deformation among all other geometries. In contrast, the triangular shape has the highest deformation and has a significant difference between other three-bar shapes.

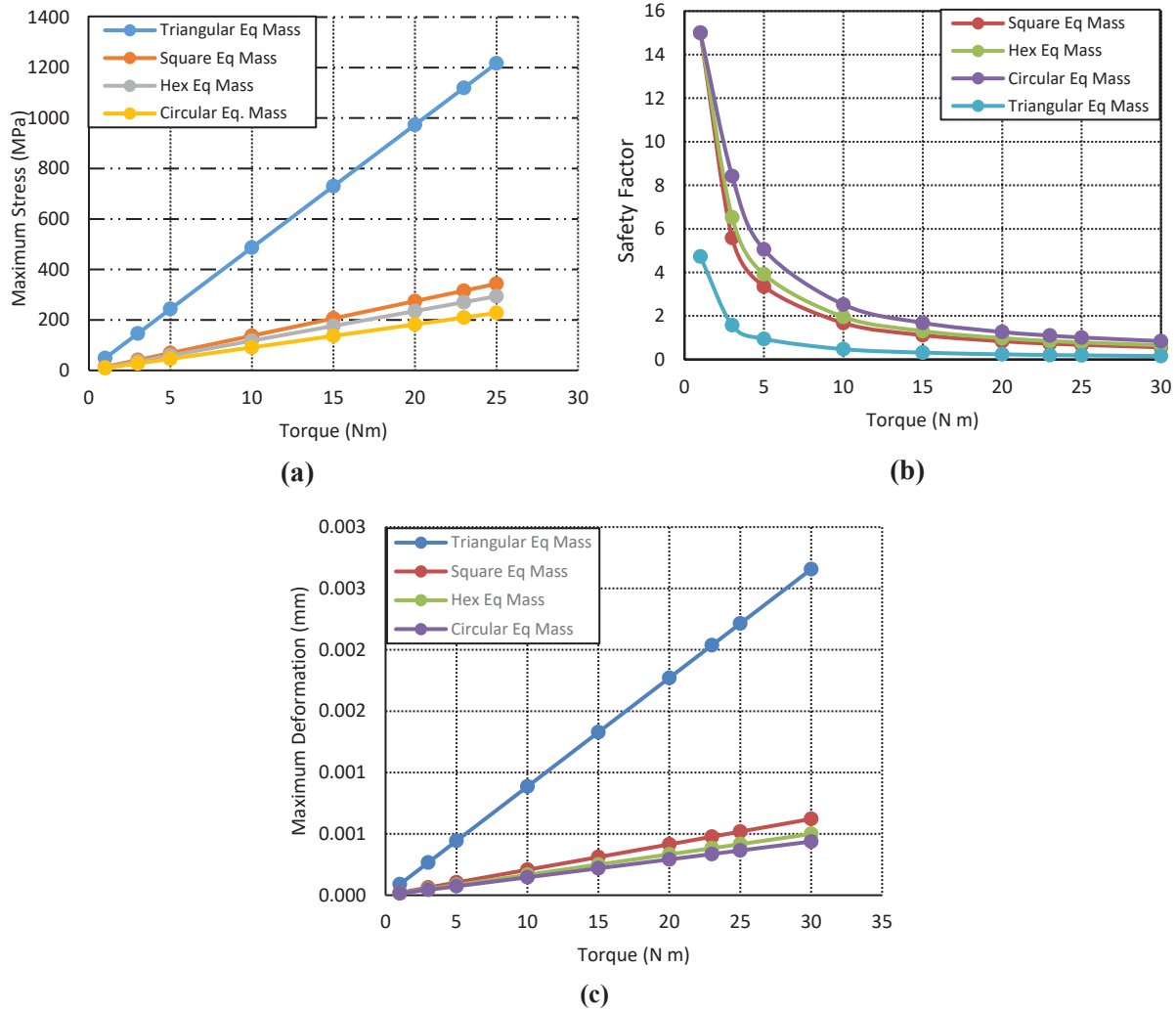
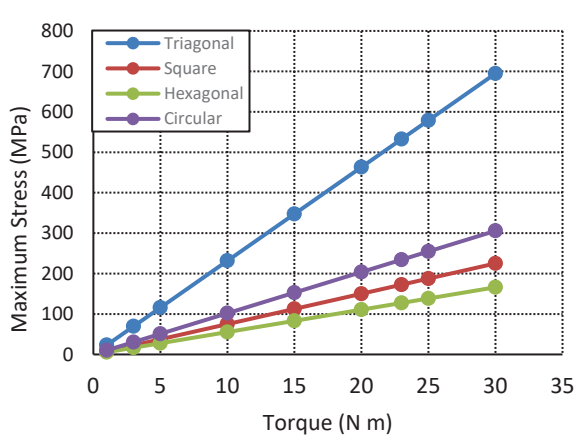


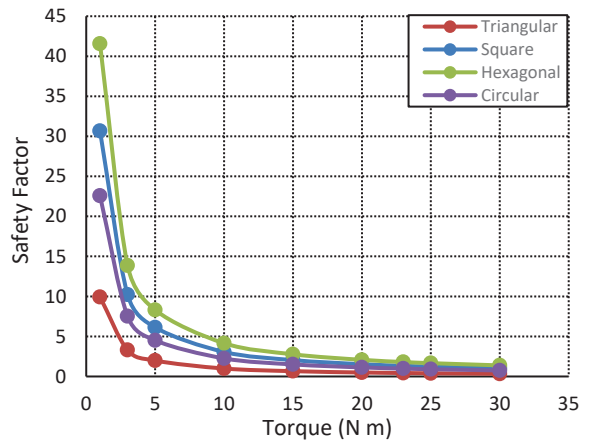
FIGURE 3. The simulation data for equal-mass cross-sectional SPCC bar (a) Maximum Stress graph, (b) Safety factor graph, and (c) Maximum deformation graph with respect to the applied torque.

The calculation for the theoretical value of maximum stress, maximum deformation, and safety factor was conducted using Microsoft Office Excel, Figures 4 (a) – (c) present the resulting calculation. **Figure 4 (a)** illustrated the stress of the bars, **Figure 4 (b)** illustrated the safety factor of different bars, and **Figure 4 (c)** illustrated the displacement or deformation of the bars. Unlike the actual results, the theoretical results show that there is a considerable difference of performance on all of the bars, shown on Figure 4 (b) (safety factor), especially on smaller loads (i.e. 5 Nm).

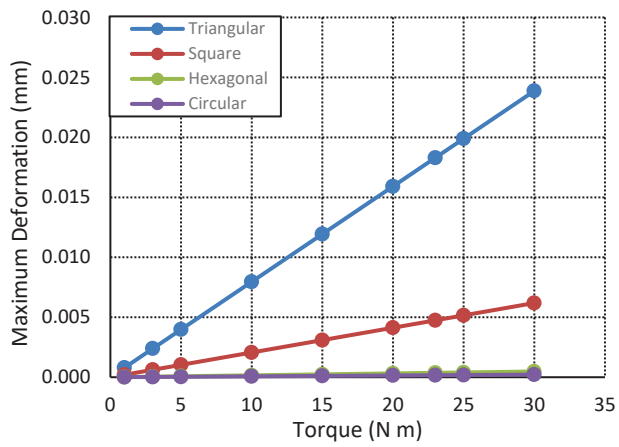
Cross-sectional figures of the simulation with equal-mass variation are presented in figure 5. **Figure 5 (a)** shows the total deformation or displacement of the bars. It is shown that the triangular bar is having the highest deformation, followed by square, hexagonal, and circular bar. **Figure 5 (b)** shows the stress of different bars. It is shown that most of the stresses concentrate on the midsection of the cross-section's sides. As the cross-section geometry gets closer to a circular shape (increasing in the number of sides), the stress gets distributed more evenly, increasing the bar's torsional strength. **Figure 5 (c)** shows the safety factor of different bars. This figure shows the same results and descriptions as **figure 5 (b)**. As shown, the triangular bar has the highest deformation, followed by square, hexagonal, and circular bar



(a)

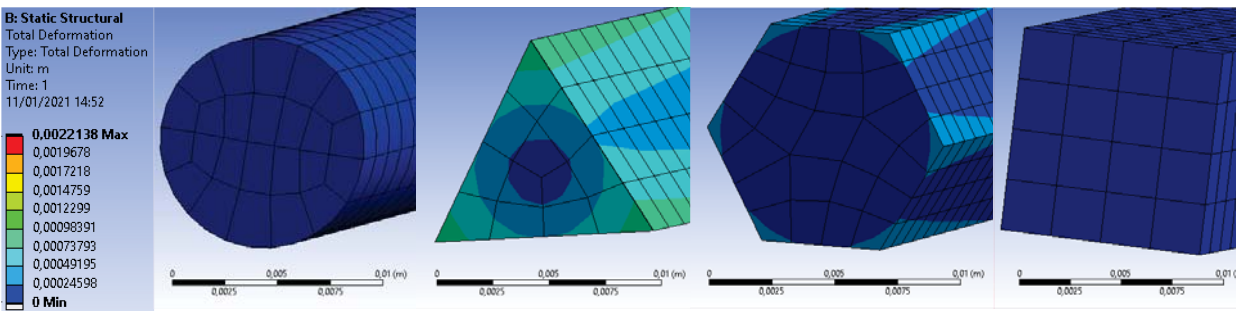


(b)



(c)

FIGURE 4. Simulation data for equal-mass cross-sectional SPCC bar. (a) Maximum Stress graph, (b) Safety factor graph, and (c) Maximum twist deformation graph with respect to the applied torque.



(a)

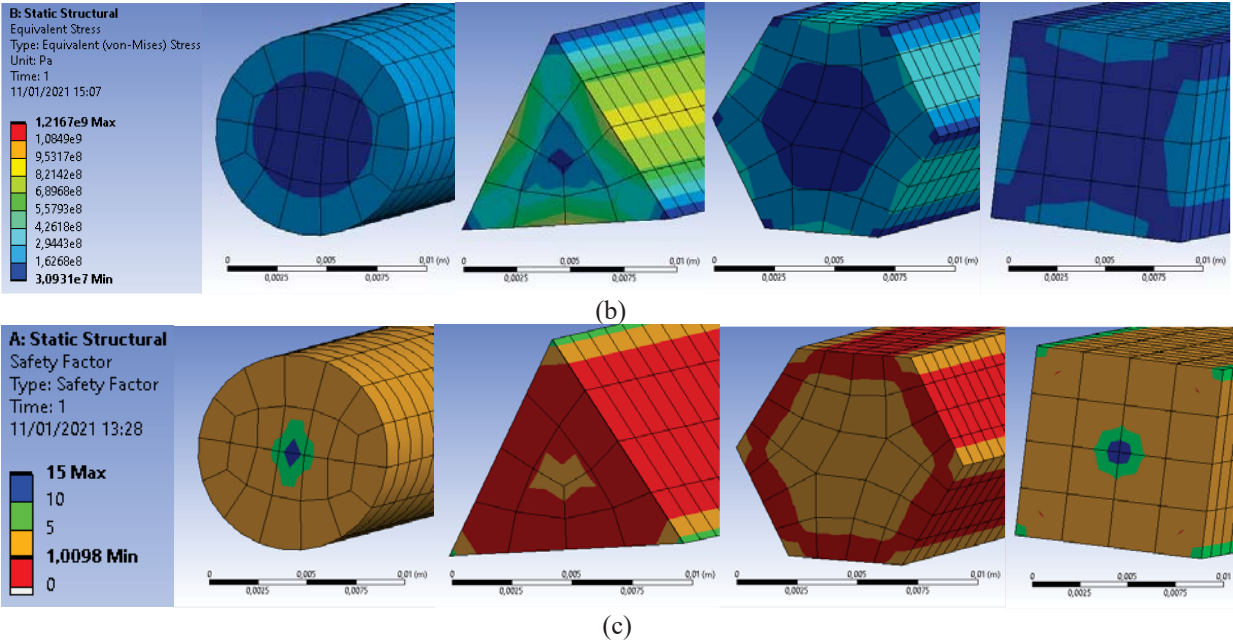


FIGURE 5. Sectional view of the simulation result of equal-mass geometrical analysis for 30 Nm torque (a) maximum twist displacement of the SPCC bar with various geometry (b) Von misses stress of the SPCC bar with various geometry (c) Safety factor of the SPCC bar with various geometry

Various Cross-Sectional Geometry with Equal Cross-Sectional Width

The simulation data with the equal-width condition is presented in Figure 6(a)-(c). Figure 6 (a) shows that the triangular bar also shows the highest stress than other geometry bars. The results also show that the square bar and the circular bar shows the negligible difference in performance. There is no significant difference between the square bar, circular bar, and hexagonal bar is lighter loads, i.e., 5 Nm. However, there is a significant difference between the triangular bar and other bars, as shown below. Figure 6 (b) illustrated the safety factor of different bars. It is shown that the safety factor on small loads (i.e., 5 Nm) of the square, hexagonal, and circular bar has a small difference. Still, the triangular bar has a substantial difference in safety factor compared to all other geometries. It also shows that the safety factor of the square and circular rod is identical on all loads. Figure 6 (c) illustrated the displacement or deformation of the bars. It is shown that the square, hexagonal, and circular rod has a small difference in displacement, with a circular shape having the lowest deformation among all other geometries. The triangular shape has the highest deformation and has a significant difference between the other three-bar shapes.

The calculation for the theoretical value of maximum stress, maximum deformation, and safety factor, Figures 7 (a) – (c) present the resulting calculation. Figure 7 (a) illustrated the stress of the bars, Figure 7 (b) illustrated the safety factor of different bars, and Figure 7 (c) illustrated the displacement or deformation of the bars. Unlike the actual results, the theoretical results show a considerable difference in performance on all of the bars, shown in Figure 4 (a) (stress), especially on larger loads, i.e., 30 Nm.

Cross-sectional figures of the simulation with equal-width variation are presented in figure 8. Figure 8 (a) shows the total deformation or displacement of the bars. It is shown that the triangular bar is having the highest deformation, followed by square, hexagonal, and circular bar. Figure 8 (b) shows the stress of different bars. It is shown that most of the stresses concentrate on the midsection of the cross-section's sides. As the cross-sectional geometry gets closer to a circular shape (increasing in the number of sides), the stress gets distributed more evenly, increasing the bar's torsional strength. Figure 8 (c) shows the safety factor of different bars. This figure shows the same results and descriptions as figure 8 (b).

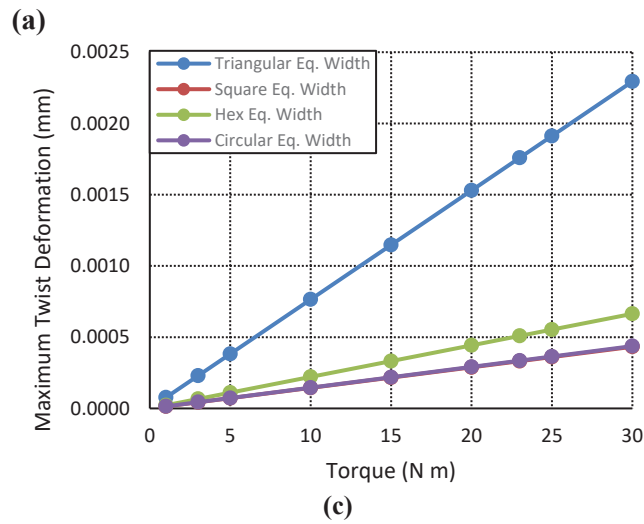
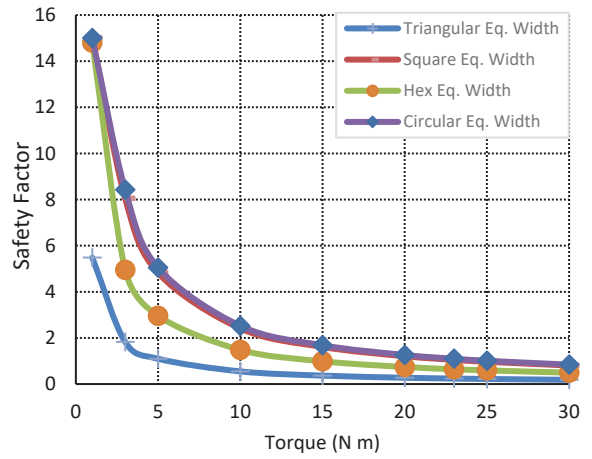
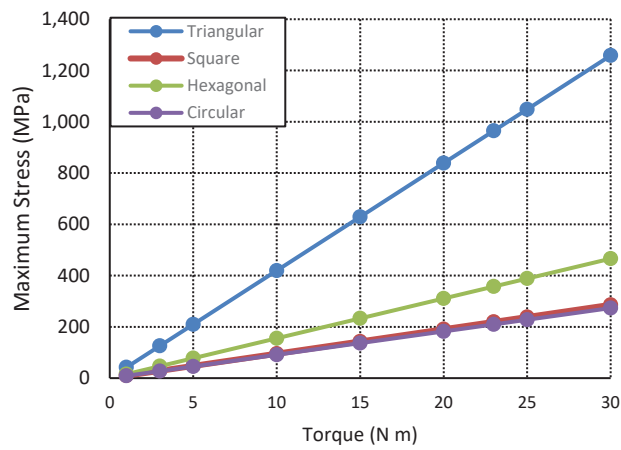
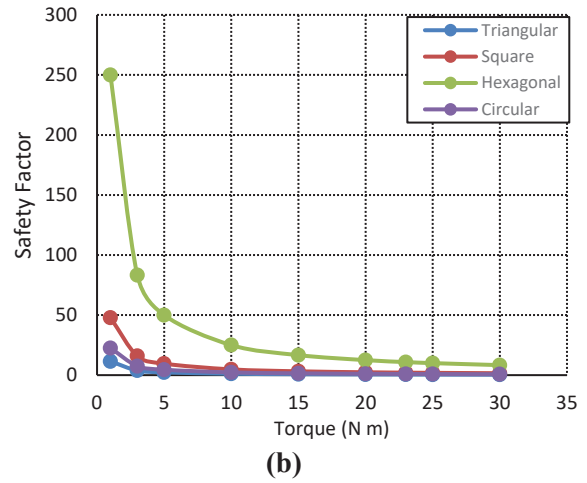
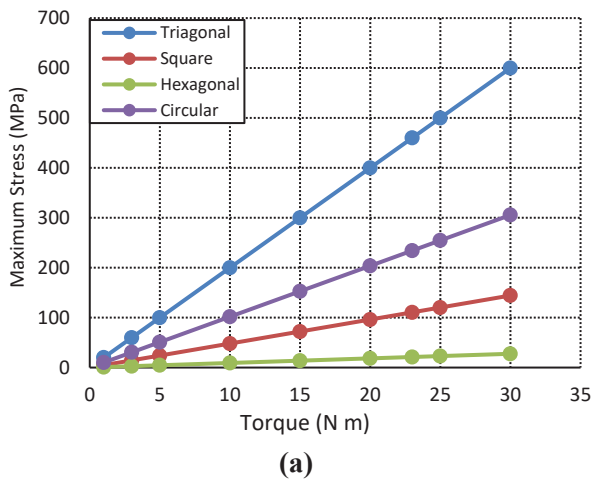
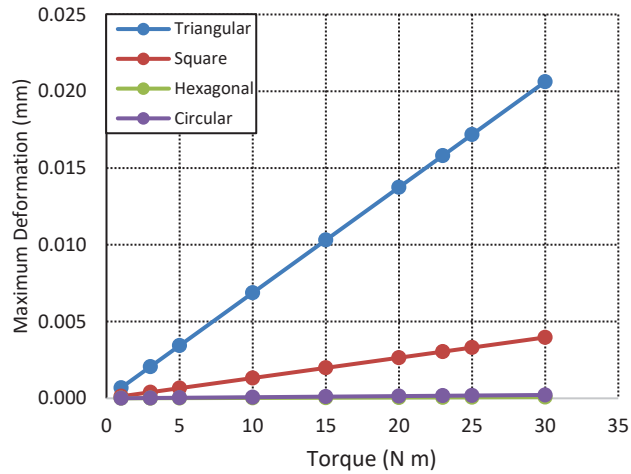


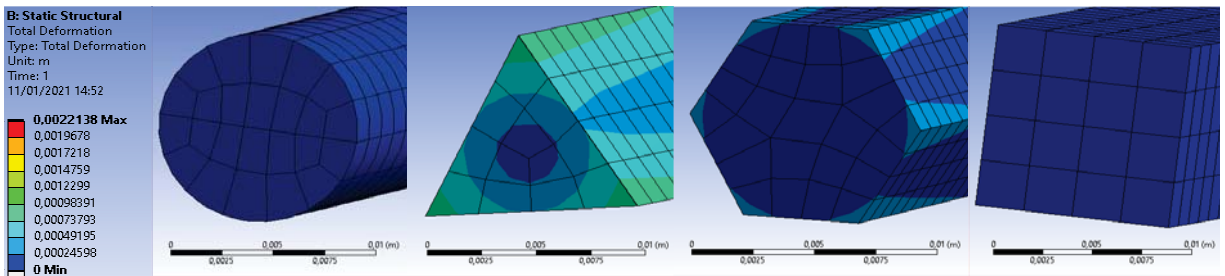
FIGURE 6. Theoretical calculation data for equal-mass SPCC bar with various cross-sectional geometry a) Maximum Stress graph, (b) Safety factor graph, and (c) Maximum deformation graph with respect to the applied torque.



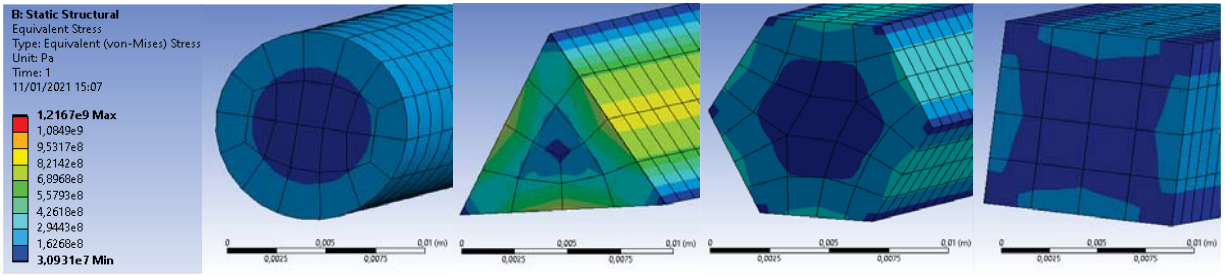


(c)

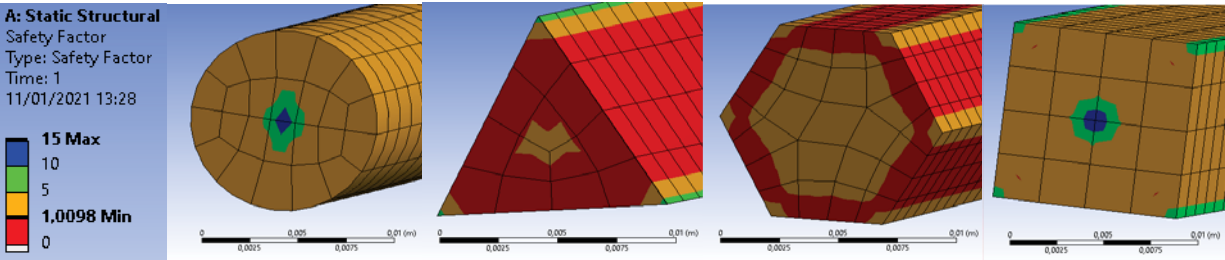
FIGURE 7. Theoretical calculation data for equal cross-sectional width SPCC bar with various cross-sectional geometry a) Maximum Stress graph, (b) Safety factor graph, and (c) Maximum deformation graph with respect to the applied torque



(a)



(b)



(c)

FIGURE 8. Sectional view of the simulation result of equal-width geometrical analysis for 30 Nm torque (a) maximum displacement of the SPCC bar with various geometry (b) Von misses stress of the SPCC bar with various geometry (c) Safety factor of the SPCC bar with various geometry

DISCUSSION

Simulations and theoretical calculations data showed an interesting effect of the SPCC bar's cross-sectional geometry on the maximum stress (von-misses stress), maximum deformation, and the SPCC bar's safety factor. Despite different methods of simulation, the result showed a very consistent trend. Figure 9 showed the maximum von misses stress obtained from simulation with equal-mass SPCC bar and equal-cross sectional width of SPCC bar. The triangular bar, in either simulation, express the largest maximum von misses stress. The result also showed that circular cross-section, despite simulation methods, consistently performed very well by showing a meagre value of maximum von-misses stress. This simulation proved that the circular geometry performed consistently well in all simulations across different torsional loading condition. This condition is observed due to the absence of the sharp edge in the circular-cross section. However, surprising behaviour is observed from square cross-sectional geometry under equal width condition. The value of von misses stress of the square approached the value of that of the circular cross-section. This condition is due to the greater polar moment of inertia of the square compared to the circular cross-section under the equal cross-sectional width condition.

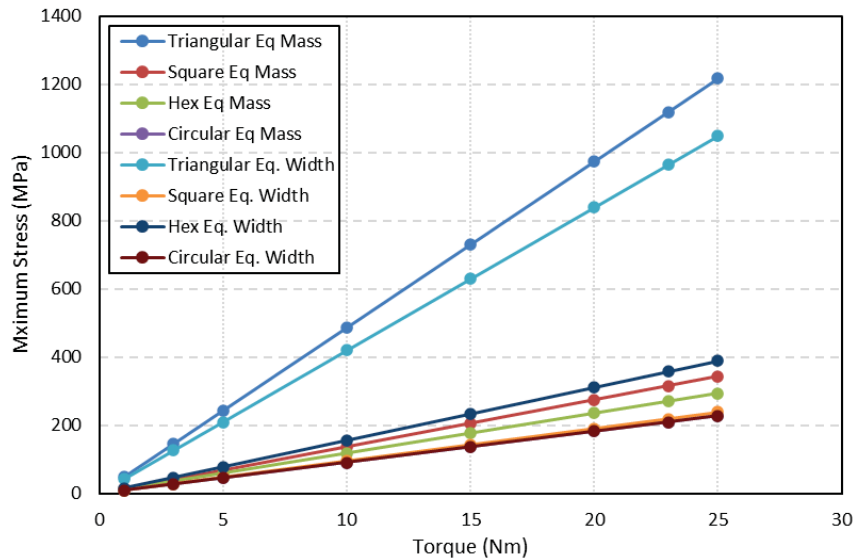


FIGURE 9. Maximum stress vs torque of all simulations

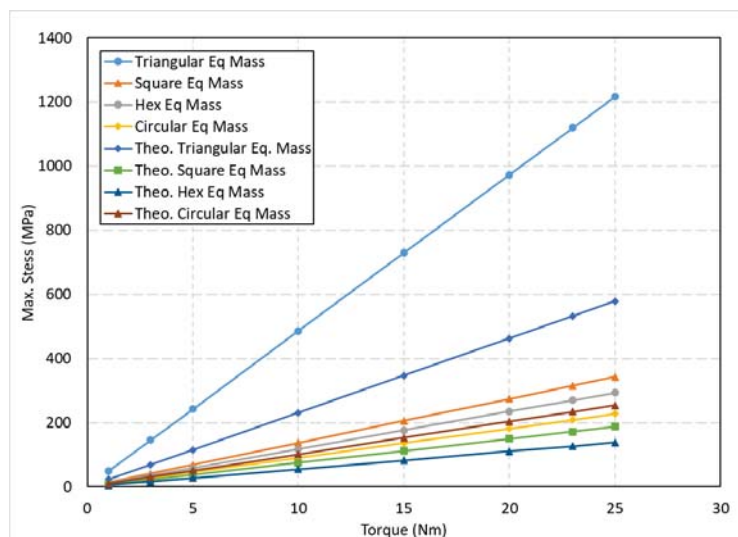


FIGURE 10. Theoretical and simulation result comparison

Comparison between the theoretical result and the simulation result is presented in the table below. Since both simulation procedures show similar trends, the equal-mass SPCC bar with various cross-sections is used to compare. Figure 8 showed a comparison between the theoretical and simulation result. The following graph shows that the value theoretical maximum stress is lower than the real maximum stress value. This condition is due to the unsymmetrical effect of the cross-sectional geometry.

Obtaining the safety factor value from the cross-sectional geometry, all of the simulation data from the equal mass and equal-width simulation. Figure 9 This figure showed that the circular geometry still presented the highest safety factors from all geometries. However, the equal-width square cross-section presented the second-highest safety factors from various cross-sectional geometry. This condition is due to the low polar moment of inertia of the square cross-sections.

Reflecting from the result, figure 10 showed a comprehensive graph of the lowest safety factors and highest displacement. In figure 10, the horizontal axis represents geometrical cross-section. From figure 10, it is shown that rounder geometries. It is shown that rounder and edgeless geometries have higher safety factors and lower maximum displacement. By using this data, engineers and designers will consider the geometrical effect on torsion application. Also, this graph shows that sharper geometry will reduce the torsional strength of the SPCC bar.

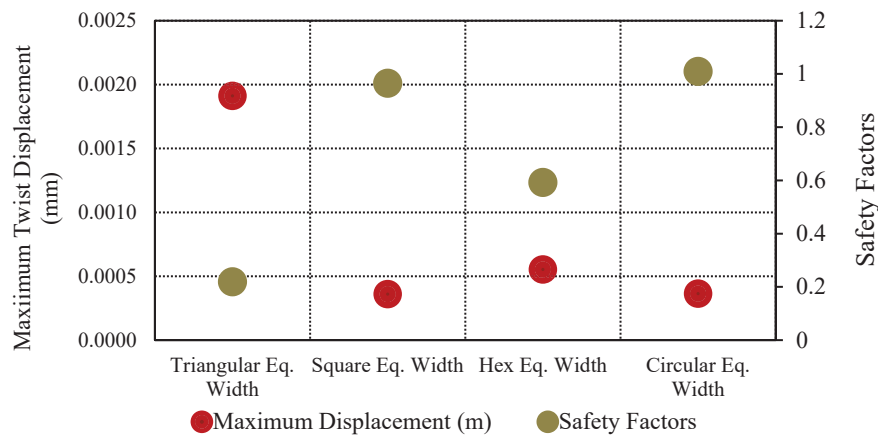


FIGURE 11. Safety factors vs maximum displacement

CONCLUSION

This research aims to develop and studied the effect of cross-sectional geometries of the SPCC bar on the maximum stress or von mises stress, maximum deformations, and the safety factor across the SPCC bar. The research also aimed to search for optimal cross-sectional geometry for the structural application. From this research, it can be concluded as follow:

1. Circular shape considered to be the best performer and the most optimal shape for torsional application over all other shapes on both groups on simulations.
2. The triangular shape is considered the worst performer over all other shapes on both groups, both from calculations and simulations.
3. While the square and hexagonal rods performed better than circular rods on calculations, both performed worse than circular rods. This condition is most likely due to stress concentration occurring on each side.
4. On simulations, rods with the increasing number of sides showed better performance, as the stresses were distributed on more sides.
5. On simulations, stress concentration occurred along each side on the midsection. Corners did not contribute as much on bearing the load.
6. On the equal width group, the square rod did not perform better the circular rod, even though the square rod had more mass and volume.

ACKNOWLEDGEMENTS

The authors want to thank the Department of Mechanical and Industrial Engineering, Gadjah Mada University, for the support as well as Aun Seed Net ASP-R 2021, Hibah RTA 2021 UGM, and Hibah DTMI 2021 for the funding.

REFERENCES

1. M.A. Muflikhun, R. Higuchi, T. Yokozeki, and T. Aoki, *Compos. Part B Eng.* **185**, 107747 (2020).
2. S. Tabrizi, H. Kazem, S. Rizkalla, and A. Kobayashi, *Constr. Build. Mater.* **95**, 748 (2015).
3. E.G. Nisbett, (n.d.).
4. S. Keeler and M. Kimchi, *Advanced High-Strength Steels Application Guidelines V5* (WorldAutoSteel, 2015).
5. T. V Galambos and A.E. Surovek, *Structural Stability of Steel: Concepts and Applications for Structural Engineers* (Wiley Online Library, 2008).
6. H. Ju, K.S. Kim, D.H. Lee, J.H. Hwang, S.H. Choi, and Y.H. Oh, *Compos. Struct.* **129**, 143 (2015).
7. T.D.G. Rao and D. Rama Seshu, *Cem. Concr. Compos.* **27**, 493 (2005).
8. W. Da Wang, Z.L. Jia, Y.L. Shi, and E.L. Tan, *J. Constr. Steel Res.* **173**, 106271 (2020).
9. A.J. Wang and D.L. McDowell, *Int. J. Solids Struct.* **40**, 2085 (2003).
10. X. Cao, L. Wu, and Z. Li, *Eng. Struct.* **209**, 109980 (2020).
11. C. Cui, Q. Yu, W. Wang, W. Xu, and L. Chen, *Vacuum* 109874 (2020).
12. X. Hu, Y. Zheng, G. Sun, X. Zhang, J. Tian, P. Wang, S. Xu, and F. Zhou, *Compos. Sci. Technol.* **201**, 108515 (2020).
13. A. Meram and A. Can, *Compos. Part B Eng.* **176**, 107142 (2019).
14. Z.B. Pi, M. Su, Y.Y. Peng, Y.H. Wang, W. Luo, and Y. Sen Lan, *Eng. Struct.* **216**, 110761 (2020).
15. Y. Yogo, M. Sawamura, N. Iwata, and N. Yukawa, *Mater. Des.* **122**, 226 (2017).
16. M.Y. Alabdulhady, L.H. Sneed, and C. Carloni, *Eng. Struct.* **136**, 393 (2017).
17. A. Hadhood, M.G. Gouda, M.H. Agamy, H.M. Mohamed, and A. Sherif, *Eng. Struct.* **206**, 110174 (2020).
18. N.A. Siddiqui, S.U. Khan, and J.K. Kim, *Compos. Struct.* **104**, 230 (2013).
19. M.A. Muflikhun and A.Y. Chua, *Data Br.* **29**, (2020).
20. M.A. Muflikhun, R. Higuchi, T. Yokozeki, and T. Aoki, *Compos. Part B Eng.* **172**, 262 (2019).
21. D. McClaflin and A. Fatemi, *Int. J. Fatigue* **26**, 773 (2004).
22. A.R. Hassani and R.T. Faal, *Int. J. Solids Struct.* **52**, 165 (2015).
23. A.R. Hassani and M.M. Monfared, *Int. J. Mech. Sci.* **128–129**, 23 (2017).
24. M.A. Muflikhun, T. Yokozeki, and T. Aoki, *Compos. Struct.* **220**, 11 (2019).
25. M.A. Muflikhun, R. Higuchi, T. Yokozeki, and T. Aoki, *Compos. Struct.* **236**, (2020).
26. S. Specification, **i**, 1 (2003).
27. R.C. Hibbeler, *Mechanics of Materials* (Pearson, 2016).
28. F. Beer and R. Johnston, *Mechanics of Materials, Eighth Edition - SI* (2020).